29th AIAA Applied Aerodynamics Conference
27 - 30 June 2011, Honolulu, Hawaii

AIAA 2011-3656

Experimental Studies on a Propelled Micro Air Vehicle

D. Arivoli[1], Ravi Dodamani[1], Roshan Antony[2], C.S. Suraj[2], G. Ramesh[1], and Sajeer Ahmed[1]
Council of Scientific & Industrial Research – National Aerospace Laboratories, Bangalore, Karnataka, 560037, India

An experimental study has been carried out on a typical Micro Air Vehicle of span 300mm having inverse Zimmerman planform. The objective is to get i) the aerodynamic characteristics of the vehicle in the range of incidence and sideslip angle the vehicle expected to encounter during its flight; ii) an understanding of the propeller effect on the aerodynamic data and iii) the control surface (elevon) effectiveness with incidence. Tests were carried out in a low speed wind tunnel at a freestream velocity of 8 m/s and 12 m/s corresponding to a test Reynolds number based on chord of about 120000 and 180000 respectively. Analysis of the aerodynamic data showed significant effect of propeller flow field on the lift, stall angle and drag of the vehicle. The propeller induced flow is seen to increase the lift coefficient at higher angle of attack and delay the stall. Nonlinear variation is observed in the rolling moment indicating the onset of asymmetric flow field at higher incidence. The effectiveness of the elevon is observed to increase linearly with incidence.

Nomenclature

C_L	=	lift coefficient
C_D	=	drag coefficient
C_M	=	pitching moment coefficient
C_S	=	side force coefficient
C_{YM}	=	yaw moment coefficient
C_{RM}	=	roll moment coefficient
$C.G$	=	center of gravity
LAR	=	low aspect ratio
Re	=	Reynolds number
V	=	velocity (m/s)
α	=	angle of attack (degree)
β	=	sideslip angle (degree)
φ	=	roll angle (degree)
δ	=	elevon deflection angle (degree)

I. Introduction

MICRO Air Vehicles (MAVs) are small class of vehicles which fly in the Reynolds number range less than 200,000 at lower atmospheric altitude in the earth's boundary layer. The small span of the wing requires larger wing area to create sufficient lift to support itself that makes it a low aspect ratio (LAR) wing. These LAR wings at low Re exhibits unique aerodynamic characteristics. Flow over the upper wing surface is prone to separation with a possible turbulent transition in the free shear layer, and then reattachment to the surface, leaving behind a separation bubble[1]. Such flow structures typically result in a loss of lift and an increased drag, which decreases the lift-to-drag ratio of the vehicle[2]. LAR wings exhibits non-linear lift. This non-linearity in lift is due to the formation of wing tip vortices which creates a low pressure on the upper surface of the wing which results in a subsequent increase in lift. These tip vortices strengthen as the angle of attack increases and might be present over most of the wing area due to which the LAR wings stalls at higher angle of attack. Destabilization of tip vortices occur beyond certain angle of attack due to its interaction with the separated flow resulting in a bilateral asymmetry which may cause rolling instabilities[3]. Controllable flight in the lower atmospheric altitude is another problem these

[1] Scientist, Experimental Aerodynamics Division., CSIR-National Aerospace Laboratories.
[2] Scientist, Propulsion Division, CSIR-National Aerospace Laboratories.

Copyright © 2011 by the American Institute of Aeronautics and Astronautics, Inc. All rights reserved.

vehicles face because the wind gust can be of the same order of magnitude as the vehicles flight speed. With all the odds these small vehicles still receives great attention because of its various civil and military applications – battle field surveillance, biochemical sensing, target tracking, traffic monitoring, etc. Extensive experimental data and limited computational data are available on the low Reynolds number, low aspect ratio wings[4,5,6]. However, while designing a new Micro Air Vehicle configuration these data can only be taken as reference but not as exact design parameters. In the design stage still one has to rely on the computational code to get a preliminary idea about the aerodynamics of the designed geometry. In addition aerodynamics of propelled model is different from the un-propelled model due to the propeller induced flow over the wing[7]. To model and solve a propeller induced flow over the MAV at design stage is a difficult task and not reliable also. Hence Micro Air Vehicles once designed have to be further optimized through wind tunnel experimentation and by flight trials. The aerodynamic characteristics of the typical Micro Air Vehicle configuration developed using a freeware software tool[8] are determined through wind tunnel tests. The basic aerodynamic characteristics of the vehicle along with the effect of propeller and elevon effectiveness are discussed in this paper.

II. Experimental Setup

A. Facility

Studies on the Micro Air Vehicle were undertaken in a closed circuit low speed wind tunnel with a test section of 2.74 x 1.83 m which has been used earlier for aerodynamic investigations in the velocity range of 8 to 50 m/s. The present studies required flow velocities to be 8 m/s and 12 m/s, and so prior to undertaking the studies, the flow in the tunnel was calibrated in this velocity range to assess its uniformity and stability. The turbulence level in this speed range is observed to be less than 0.25%.

B. Model

Figure 1 shows the dimensions of the model. The model is a high wing configuration with a modified inverse Zimmerman planform with a top and bottom vertical tail. The wing is based on S4083 airfoil's camber. The thickness of the cambered wing is 3 mm throughout a span of 300 mm. The aspect ratio of the wing is 1.46. The fuselage is of rectangular configuration with a stub front end and a boat tail at the rear. The propeller and the motor assembly was mounted on a splitter plate of 4 mm thickness which was glued to the fuselage nose. The motor is AXi 2203/46 (KV 1720) DC brushless motor and the propeller is a GWS 7"x3.5" propeller.

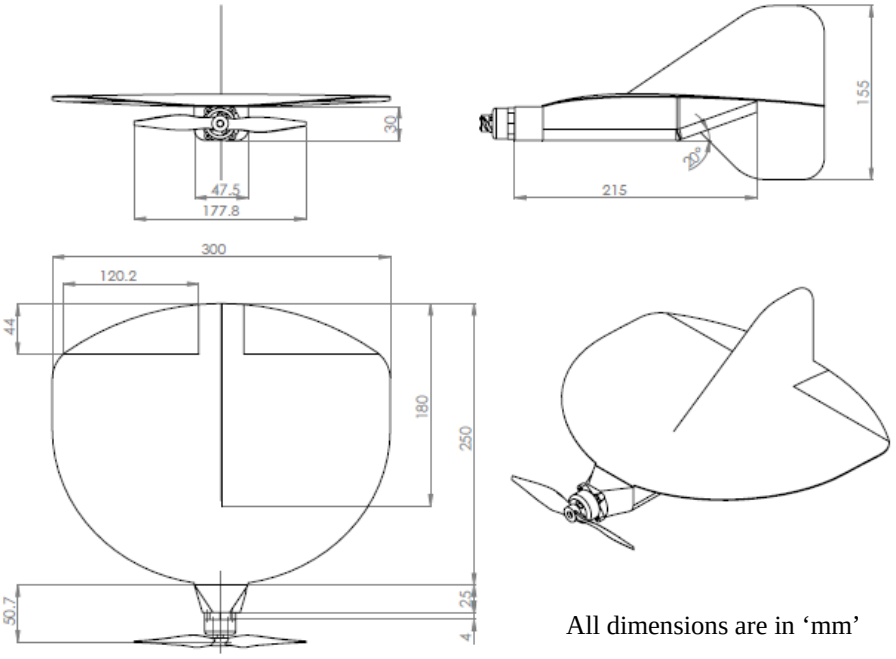

Figure 1. Dimensions of the model

C. Test Setup

The model was mounted on an internal strain gage balance supported by a vertical strut to provide clearance for bottom vertical tail. The balance was mounted on a sting from the pitching sector mechanism. Figure 2 shows the photograph of the experimental setup. Symmetric and antisymmetric elevon defections of the model was done through servos. The servos were mounted on either side of the fuselage and connected to the elevons through link rods. The servos were controlled by a control unit to desired elevon deflection angle which was placed outside the tunnel. The motor was powered by an external DC power supply from outside the tunnel and the speed of the propeller was controlled by Medusa Kit which was connected to the PC through Power PRO software.

All measurements on the model were done using a six component internal strain gage balance. Signals from the balance elements were amplified, digitized using NI based 16 bit A/D converter card and were acquired using Labview software. The acquired data from each element is averaged and converted into forces using calibration constants of the balance. The forces and moments obtained are expressed as non-dimensional coefficients and analyzed.

Figure 2. Photograph of the model mounted inside the tunnel

D. Test Conditions

Wind tunnel tests were conducted on the micro air vehicle model at a freestream velocity of 8 m/s and 12 m/s which corresponds to chord Reynolds number of 120000 and 180000. For the un-propelled (motor off) model test, the propeller was kept locked vertically and for propelled (motor on) model test, the propeller was maintained at 8000 rpm throughout the angle of attack. Tests were conducted on the model in the incidence range of -15^o to 35^o and sideslip angle of 0^o to 15^o. Control effectiveness is studied by deflecting the elevons in both symmetrical and anti-symmetrical deflection. The deflection angle ranges from -15^o to 15^o in steps of 5^o.

III. Results and Discussions

A. Comparison of lift and drag coefficients between propelled and un-propelled model

The propelled and un-propelled model was tested at two different Reynolds number at 120000 and 180000 which are based on root chord and freestream velocity. For the propelled model test at both the Reynolds number, the propeller speed was maintained at 8000 rpm. The purpose of the test is to study the effect of propulsive induced flow at different Reynolds number. Figure 3 and 4 shows the comparison of lift and drag coefficients of the propelled model with the un-propelled model. Propelled model at Re 120000 shows tremendous increase in C_L and a delayed stall angle occurring at 36^o. This shows the effective dominance of propulsive induced flow which gives a local acceleration of flow around the wing thereby increasing the pressure difference between top and bottom of the wing all the more. This increase in the pressure difference provides additional lift to the wing beyond the lift generated by the wing in un-propelled condition. Also the lift coefficient of the model under this propulsive-induced flow is non-linear beyond 20^o and upto the stall angle. With increase in Reynolds number to 180000 for the same propeller speed, the model shows a decrease in C_L and stall angle. C_{Lmax} and stall angle of the propelled model has decreased by 23% and 12% respectively from what has been observed at Re 120000.

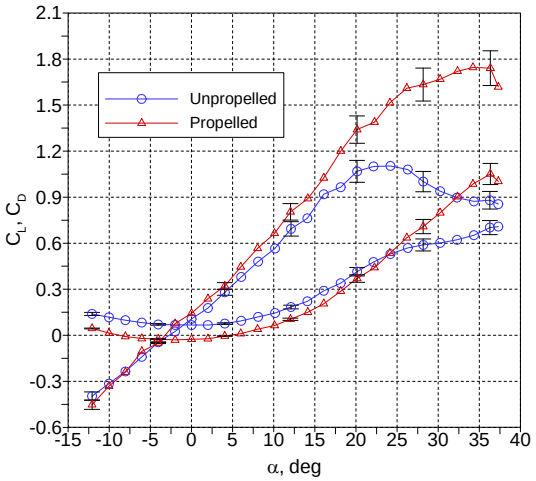

Figure 3. Comparison of lift and drag coefficient at Re=120000

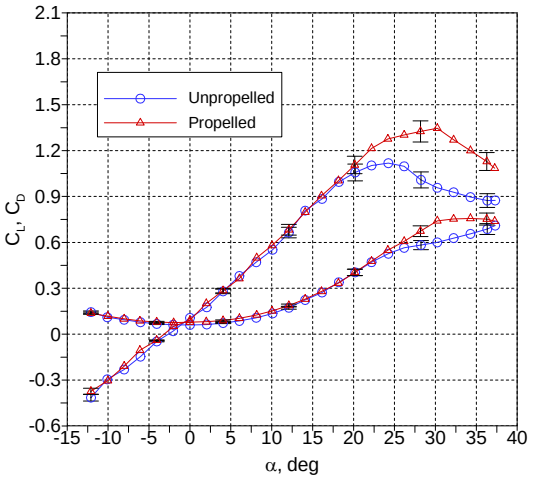

Figure 4. Comparison of lift and drag coefficient at Re=180000

Drag coefficient of the propelled model at Re 120000 shows decreased values upto 24° angle of attack. In particular to note is the negative C_D between -5° to 5° angle of attack. This decrease in C_D and also the negative C_D is due to the thrust produced by the propeller which pulls the MAV model against the freestream. The thrust and axial force are forces acting opposite to each other on the model. The balance can either measure thrust or the axial force of the model and in a condition where the both are present, the balance measures the sum of the thrust and axial force acting on the model. Therefore the C_D of the propelled model in a true sense is derived from the global forces which is the sum of the thrust and axial force acting on the model. At Re 180000, the drag coefficent of the propelled model is same as the un-propelled model. This shows that the model only experiences drag despite the propeller running at 8000 rpm. This is because as the forward velocity increases the angle of attack seen by the blades of a fixed-pitch propeller decreases. This limits the thrust obtained at higher speeds[9]. This can also be seen from Fig. 5, that as the freestream velocity increases, the thrust developed by the propeller (rotating at a constant speed of 8000 rpm) decreases.

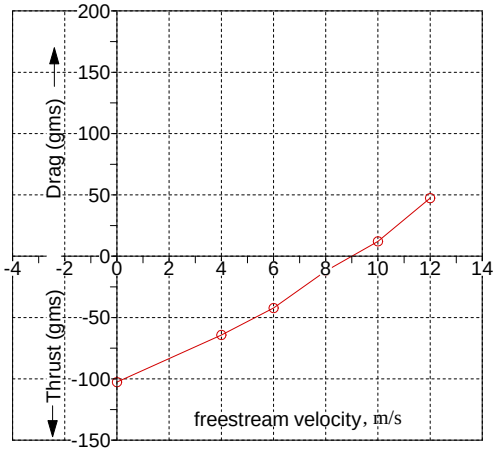

Figure 5. Thrust vs freestream velocity for the model at 0° angle of attack with the propeller running at 8000rpm

The following sections discuses the results obtained from the propelled model test at Reynolds number 180000 with the propeller running at 8000 rpm.

B. Symmetric elevon deflections of propelled model at 0° sideslip angle

Figure 6 to 8 shows the longitudinal aerodynamic characteristics for different symmetric elevon deflections ranging from -15° to 15° at 0° sideslip angle at Re 180000. Increasing trends in lift, and drag coefficients were observed with increase in elevon deflections which increases the camber of the wing. The lift slope remains constant for all deflections. C_{Lmax} increases and the zero-lift angle of attack is shifted to more negative value with increase in elevon deflection. Stall angle of the model remains constant between -5° and 5° elevon deflections. Stall is gradual for negative elevon deflection and little abrupt for positive deflections. Though the drag coefficient of the model at 0° angle of attack is almost same for all elevon deflections, with increase in angle of attack it shows progressive increase for increasing elevon deflections. This progressive increase in C_D is due to the increase in lift induced drag with increase in camber of the wing. The variation of pitching moment coefficient with respect to angle of attack shown in Fig. 8 is about the computed C.G. location. For 0° elevon deflection, it shows negative values throughout the angle of attack range which indicates a nose down pitching moment. This clearly shows that the center of pressure lies behind the C.G. The nose down pitching moment is nearly constant from -6° to 15° beyond which it increases more negative upto 30° showing a negative slope. All the elevon deflections shows a similar trend. C_M

values which corresponds to -15° elevon deflection shows positive moment values upto 20° angle of attack. Since the current C.G. location gives nose down pitching moment for the entire angle of attack range, its location needs to be adjusted in the longitudinal axis by appropriate placement of components inorder to get a trim at the design cruise angle of attack.

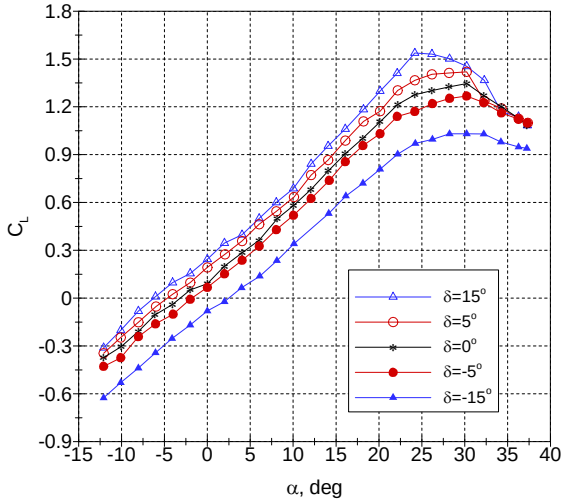

Figure 6. Lift coefficient with respect to symmetric elevon deflection at Re=180000

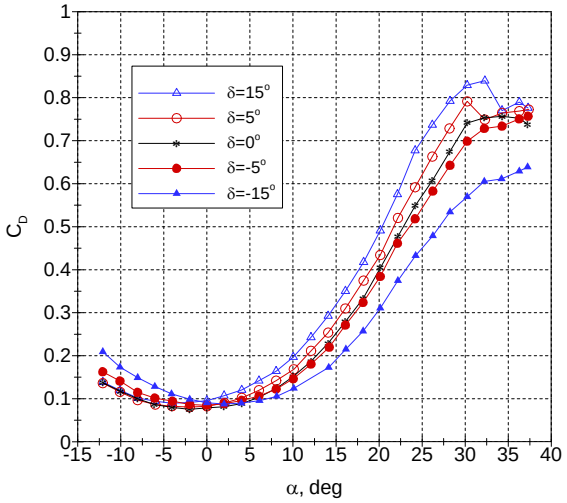

Figure 7. Drag coefficient with respect to symmetric elevon deflection at Re=180000

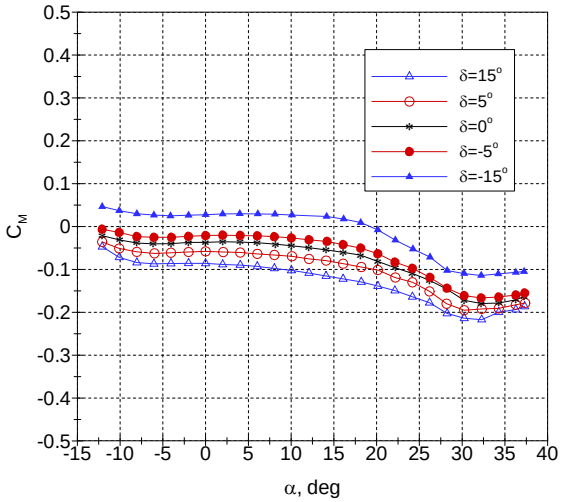

Figure 8. Pitching moment coefficient with respect to symmetric elevon deflection at Re=180000

Symmetric elevon deflections show negligible effect on side force and yawing moment – Fig. 9 and 10. The side force during a pitch angle sweep at 0° sideslip angle should be nearly zero but the measurement shows a scatter around zero. This might be caused due to the minor asymmetry of the model, small deviation of thrust line from the model longitudinal axis, the alignment of the model in the tunnel, or the calibration of the sting balance all of which are inherent to any type of measurement. From Fig. 11, though the roll moment which is supposed to be zero at 0° sideslip of the model, it shows a scatter around zero upto 10° beyond which it starts to show significant increase and attains a maximum at around 28° angle of attack near the stall. Roll moment due to reaction torque which is inherent to single propeller driven engines is not seen here in the flying range upto 10° angle of attack or the magnitude is within the range seen here. The increase in roll moment beyond 10° angle of attack might be due to the separated regions above the wing becoming bilateral asymmetric[3] due to the interaction of the wing tip vortices with the separated flow.

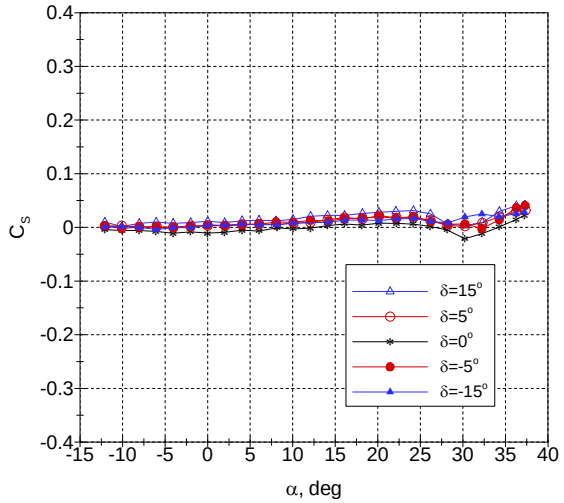

Figure 9. Side force coefficient with respect to symmetric elevon deflection at Re=180000

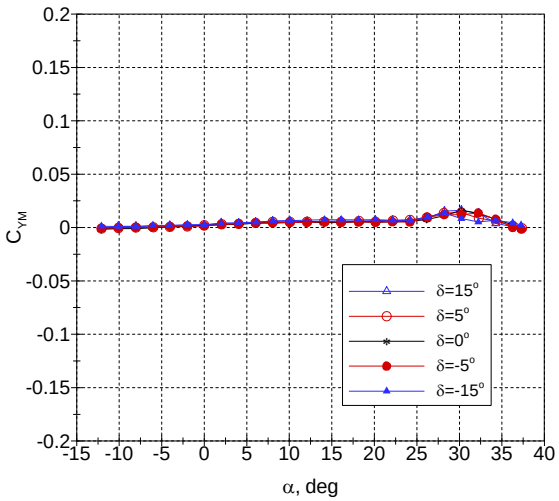

Figure 10. Yaw moment coefficient with respect to symmetric elevon deflection at Re=180000

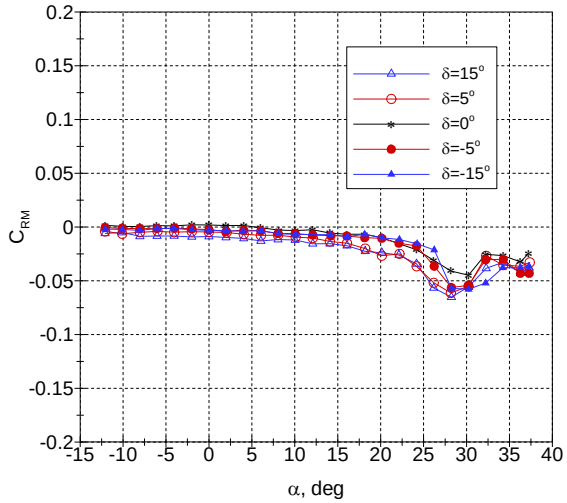

Figure 11. Roll moment coefficient with respect to for symmetric elevon deflection at Re=180000

C. Antisymmetric elevon deflections of propelled model at 0° sideslip angle

Figure 12 shows the lift and drag characteristics of the model for different antisymmetric elevon deflections at 0° side slip angle. To check for the symmetric behavior of the model in the longitudinal axis, experiment was conducted at antisymmetric elevon deflection of (15°, -15°) in addition to the deflection (-15°, 15°). The lift, drag and pitching moment coefficient shows no significant change with the antisymmetric elevon deflection upto the stall angle of attack. The loss in lift and reduction in drag due to the reflex created by the negative deflection of elevon might be compensated by the increase in lift and drag due to the increase in camber of the wing created by positive elevon deflection.

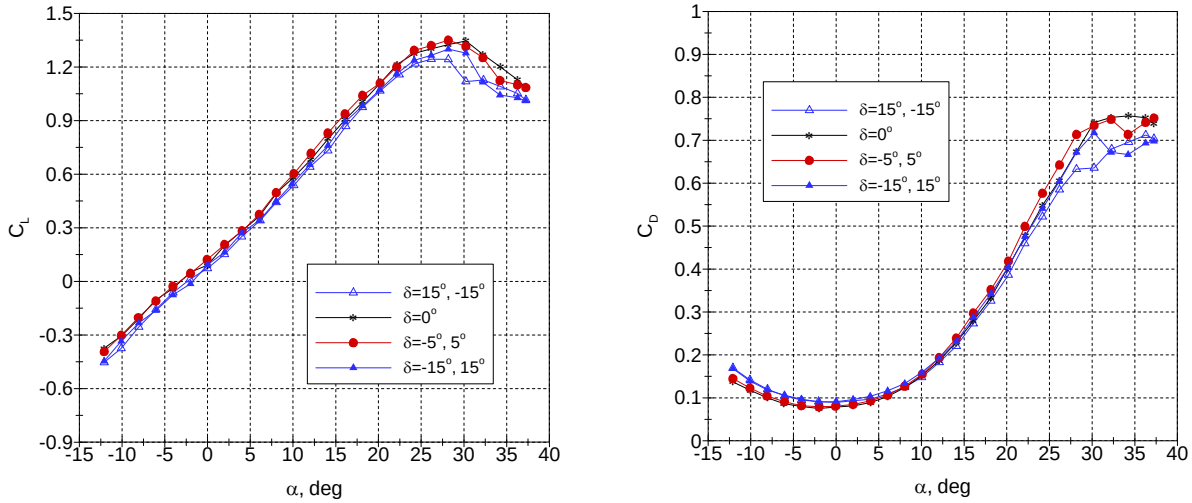

Figure 12. Lift coefficient (left) and drag coefficient (right) with respect to antisymmetric elevon deflection at Re=180000

Figure 13 shows the yaw and roll moment characteristics of the model for different antisymmetric elevon deflections at 0^o side slip angle. Antisymmetric elevon deflections shows negligible effect on yaw moment up to 20^o angle of attack. The roll moment shows increasing trends with increase in antisymmetric elevon deflections. A good symmetry in the roll moment coefficient is also observed for the antisymmetric elevon deflection between (-15^o,15^o) and (15^o,-15^o). Yaw moment associated with the antisymmetric elevon deflection is not seen here.

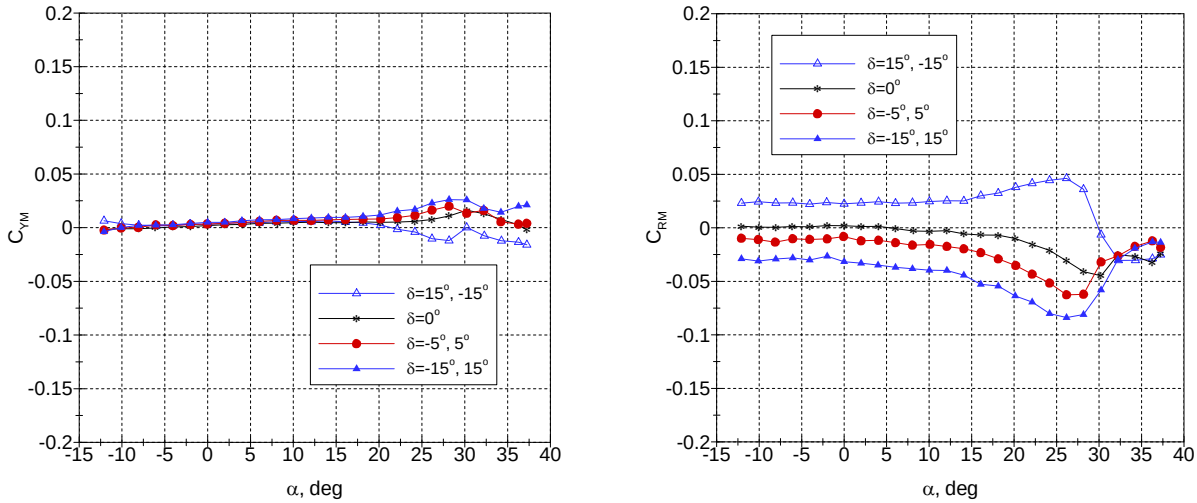

Figure 13. Yaw moment (left) and roll moment (right) coefficient with respect to antisymmetric elevon deflection at Re=180000

D. Effect of sideslip angle – propelled model

To asses the aerodynamic behavior of the vehicle during cross wind shear which may change its sideslip angle, the experiments were conducted at 5^o, 10^o and 15^o sideslip angle keeping the elevon undeflected at 0^o. Figure 14 shows the comparison of C_L, and C_D at different sideslip angles at Re=180000. Lift coefficient did not show any significant change with respect to the sideslip angles tested. Drag coefficient shows a subsequent increase upto 20^o angle of attack with increase in sideslip angle. This may be due to the increase in resolved component of force acting along the longitudinal axis experienced by the vertical tail due to its inclination to the freestream at the sideslip angles.

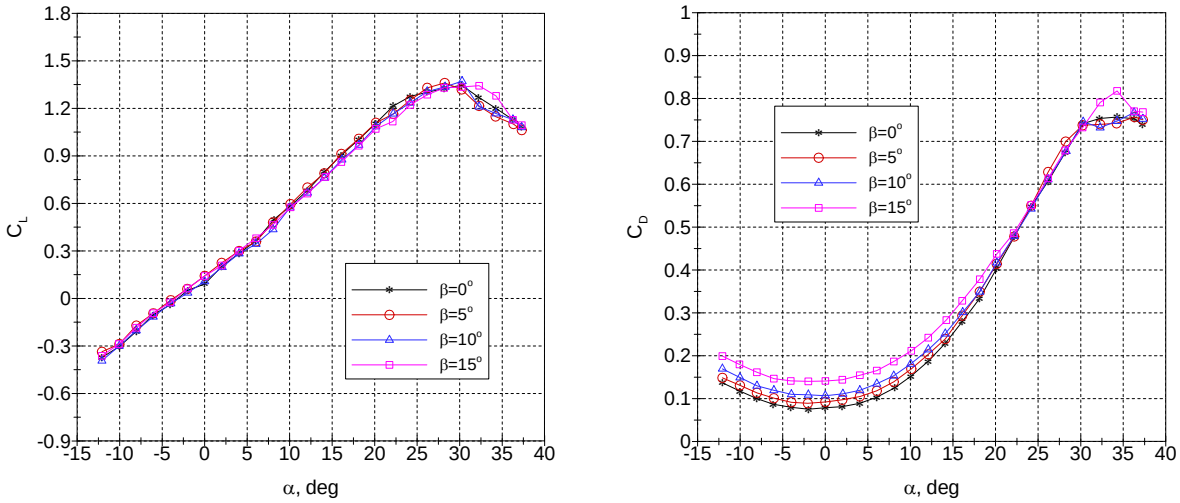

Figure 14. Lift coefficient (left) and drag coefficient (right) with respect to sideslip angles at Re=180000

The yaw and roll moment coefficient versus angle of attack for the model at 0^o elevon deflection at different sideslip angles shows some interesting trends – Fig. 15. Increasing trends in yaw moment coefficient is observed for the sideslip angles from 5^o to 15^o. For the sideslip angles tested, a constant yaw moment is observed for angles of attack upto 20^o incidence, beyond which it decreases. This decrease in yaw moment might be due to the vertical tail which is the main source of side force and roll moment is getting camouflaged behind the wing with increase in angle of attack. Roll moment variation show mixed trend of positive and negative slope for pitch angle sweep for every sideslip. This mixed trend might be associated with the onset of asymmetric flow on the model.

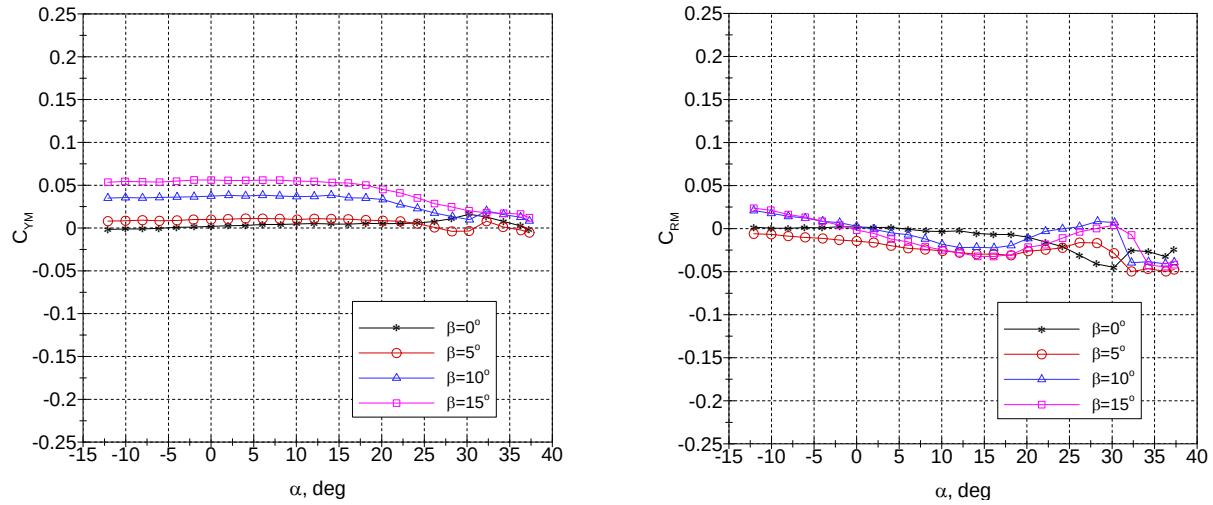

Figure 15. Yaw moment (left) and Roll moment (right) coefficients at sideslip angles at Re=180000

Figure 16 depicts the yaw moment and roll moment coefficient for the model at 0^o elevon deflection for 0^o, 6^o and 10^o angles of attack. The yaw moment curve exhibits a positive slope which implies positive directional stability of the vehicle – a perturbation in sideslip will cause a restoring yawing moment. The model exhibits non-linear roll moment characteristics with increase in sideslip angle.

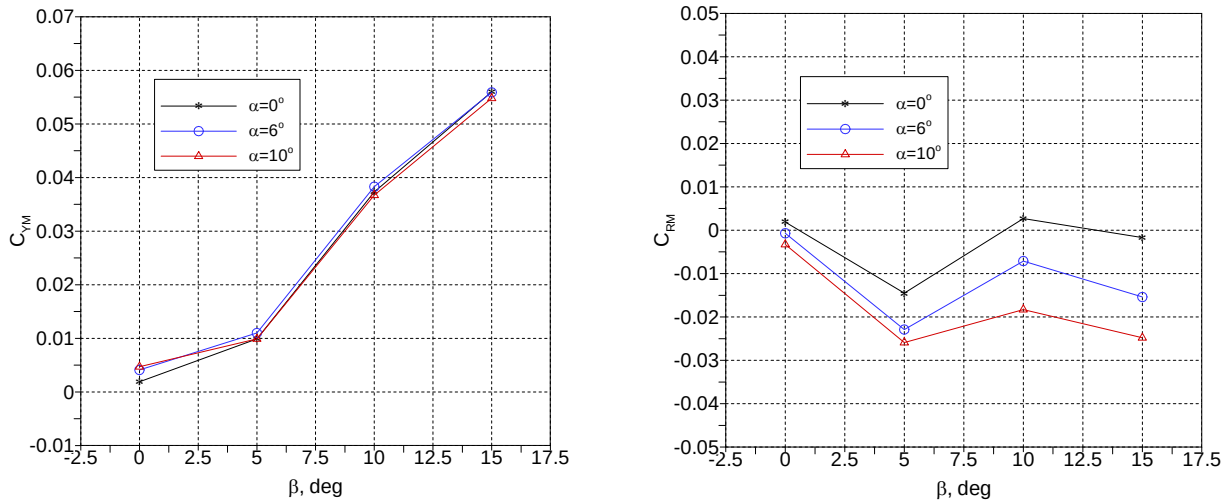

Figure 16. Effect of sideslip angle on yaw moment (left) and roll moment (right) characteristics at Re=180000

E. Effect of roll angle – propelled model

To obtain the stability of the vehicle in the lateral direction and the associated directional characteristics, the model was rolled to 25° and experiments were conducted. Figure 17 shows the roll moment and associated yaw moment characteristics of the model at 25° roll angle of the model. The model exhibits an increasing anticlockwise roll moment with increasing pitch angle sweep. The yaw moment of the model associated with the roll angle shows a typical behavior . It is constant between -10° and 5° in the positive direction, beyond which it decreases, drops to zero moment and starts to increase in the opposite direction upto 34°. The changing incidence of the vertical tail with respect to the freestream throughout the pitch angle sweep might be a reason for this behavior.

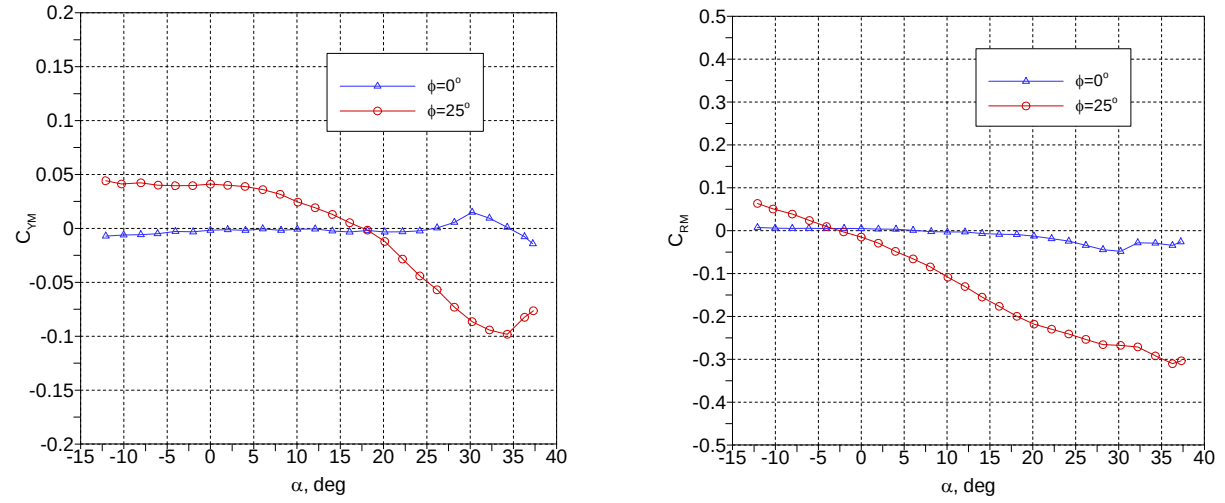

Figure 17. Efect of roll angle on yaw moment (left) and roll moment (right) characteristics at Re=180000

F. Uncertainty and blockage

Uncertainties in the measurements were computed using Kline-McClintock technique[10] for error propagation. The uncertainty calculation in the coefficients is based on RSS (Root Sum of Squares) type uncertainty. The uncertainty in coefficients is found to be around 7% of the measured value at every point. Figure 18 shows the uncertainty levels in the coefficients at Re=180000. No blockage corrections were applied to the data as the blockage factor in the tunnel is less than 1%.

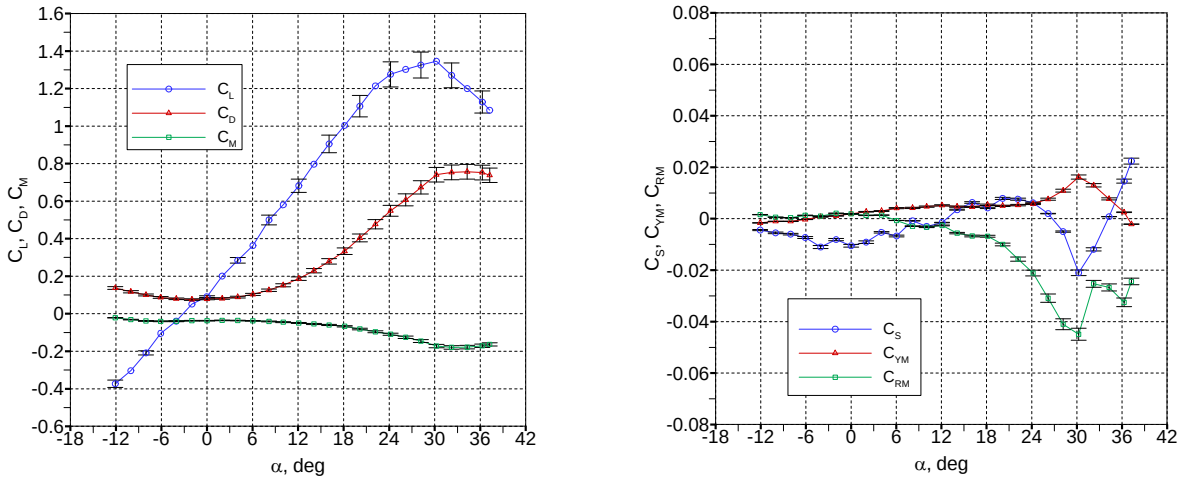

Figure 18. Uncertainty levels in measurement at Re=180000

IV. Conclusion

Experiments were conducted on a full scale model of Micro Air Vehicle of span 300mm in propelled and un-propelled condition at two different Reynolds numbers 120000 and 180000. The objective is to get an understanding of the effects of Reynolds number, propulsive induced flow, and control surface effectiveness. Analysis of the data revealed the presence of propulsive induced flow increases the lift coefficient and delay the stall to a greater extent. Increase in Reynolds number cause the effect of propulsive induced flow to decrease. The model exhibits almost a linear response with symmetric elevon deflection. Rolling moment variation showed nonlinearity at higher incidence angles due to onset of asymmetric flows. Adverse yaw effect associated with the roll in antisymmetric elevon deflection is not seen, as the model is stable in the directional axis.

Acknowledgements

The authors would like to thank Dr.L.Venkatakrishnan, Head, Experimental Aerodynamics Division for his valuable comments and suggestions. The authors also acknowledge the support of the low speed tunnel staff.

References

[1]Young, A. and Horton, H. "Some results of investigation of separation bubbles," *AGard Conf proc*, 1966(4):779-811.

[2]Torres, G., "Aerodynamics of Low Aspect Ratio Wings at Low Reynolds Number with applications to Micro Air Vehicle Design," Ph.D. Dissertation, Department of Aerospace and Mechanical Engineering, University of Notre Dame, South Bend, IN, 2002.

[3]Tang, J., Zhu, K., "Numerical and Experimental Study of Flow Structure of Low Aspect Ratio Wing," *Journal of Aircraft*, Vol. 41, No. 5, September-October 2004, pp. 1196-1201.

[4]Zimmerman, C. H., " Aerodynamic Characteristics of several Airfoils of Low Aspect Ratio", NACA Technical Note No.539, Washington, 1935

[5]Torres, G. E., and Mueller, T. J., "Low-Aspect-ratio wing aerodynamics at Low Reynolds Numbers," *AIAA Journal*, Vol. 52, No.5, May 2004.

[6]Mueller, T. J., "Fixed and Flapping Wing Aerodynamics for Micro Air Vehicles," *AIAA progress in Astronatics and Aeronautics*, Vol.195, 2001.

[7]Null, W., Noseck, A., and Shkarayev, S., "Effects of Propulsive-Induced Flow on the Aerodynamics of Micro Air Vehicle," *23rd AIAA Applied Aerodynamic Conference,* 6-9 June 2005, Toronto, Ontario, Canada.

[8]XFLR5, Software Package, Ver. 3.19, MIT, Cambridge, MA, 2006.

[9]Raymer, P., *Aircraft Design: A Conceptual Approach*, American Institue of Aeronautics and Astronautics, Inc., Washington, D.C. 20024

[10]Kline, S. J., and McClintok, F. A., "Describing Uncertainties in Single-Sample Experiments," *Mechanical Engineering*., Vol.75, No.1, January 1953:3-8.